Submitted to Annual Review of Nuclear and Particle Science 2016

Long-Baseline Neutrino Experiments

M. V. Diwan
Brookhaven National Laboratory, Upton, NY, USA

V. Galymov
Institut de physique nucléaire de Lyon, Villeurbanne, France

X. Qian
Brookhaven National Laboratory, Upton, NY, USA

A. Rubbia
ETH Zurich, Institute for Particle Physics, Zurich, Switzerland

Abstract We review long-baseline neutrino experiments in which neutrinos are detected after traversing macroscopic distances. Over such distances neutrinos have been found to oscillate among flavor states. Experiments with solar, atmospheric, reactor, and accelerator neutrinos have resulted in a coherent picture of neutrino masses and mixing of the three known flavor states. We will summarize the current best knowledge of neutrino parameters and phenomenology with our focus on the evolution of the experimental technique. We will proceed from the first evidence produced by astrophysical neutrino sources to the current open questions and the goals of future research.

CONTENTS

Introduction 2

The Three-flavor neutrino Standard Model 6
Measurement of $|\Delta m^2_{32}|$ and θ_{23} 7
Measurement of Δm^2_{21} and θ_{12} 9
Measurement of θ_{13} 11

Phenomenology of CP violation and mass hierarchy 13

Current-generation of Experiments 16

Next-generation Experiments 18
Atmospheric Neutrinos 18
Reactor Neutrino Oscillations 18
Accelerator Neutrino Oscillations 20

Conclusion 22

1 Introduction

Neutrinos are electrically neutral spin-1/2 particles that are emitted in radioactive decays of unstable nuclei and subatomic particles. They were originally proposed by W. Pauli in 1930 (1) as an explanation of the apparent non-conservation of energy in radioactivity and inconsistencies between the exclusion principle and nuclear models of that time. Enrico Fermi was responsible for the modern name of the particle and the theory of beta decay which is the foundation for current understanding of weak interactions (2). Soon after the detection of free neutrinos from radioactive products in nuclear reactors (3,4), neutrino properties and their fundamental role in shaping the universe became an important line of inquiry (5, 6).

Important questions regarding neutrinos are: the number and types of neutrinos, the nature and strength of their interactions with matter, their masses, and the origin of these masses. A series of ground breaking experimental observations and theoretical advances since the 1950s have made progress on these issues (7). While neutrino physics historically had been synonymous with understanding of weak interactions, the observation of neutrino oscillations has opened a new portal to fundamental questions regarding the relationship between quarks and leptons and the origin of fermion masses (8).

After the detection of neutrinos from nuclear reactors, the hypothesis of neutrino-antineutrino mixing was made in analogy to neutral mesons (9,10) given that only one type of neutrino was known at that time. This hypothesis was naturally extended to mixing of neutrino flavors (11–13), when the neutrinos produced in pion decays from a proton accelerator were shown to be distinct from neutrinos produced in beta decays (14). Subsequently, the mixing of fields was realized to be a natural consequence of gauge theories with spontaneous symmetry breaking. Both quarks and neutrinos have now been shown to experience flavor mixing although possibly originating from different mechanisms since neutrinos do not have electric charge. Whereas quarks and charged leptons are Dirac fermions with oppositely charged anti-particles, neutrinos could be either Dirac type with a conserved leptonic charge or neutral Majorana particles with no conserved leptonic charge.

Under the simplest assumption of two-flavor neutrino mixing characterized by a single angle θ, ν_e and ν_μ are superpositions of two mass eigenstates ν_1 and ν_2 with masses m_1 and m_2:

$$\begin{pmatrix} \nu_e \\ \nu_\mu \end{pmatrix} = \begin{pmatrix} \cos\theta & \sin\theta \\ -\sin\theta & \cos\theta \end{pmatrix} \cdot \begin{pmatrix} \nu_1 \\ \nu_2 \end{pmatrix}. \tag{1}$$

The time evolution of the ν_μ state in vacuum in terms of E_1 and E_2, the energies of the two mass eigenstates, is given by:

$$\nu_\mu(t) = -\sin\theta \cdot e^{-iE_1 \cdot t} \cdot \nu_1 + \cos\theta \cdot e^{-iE_2 \cdot t} \cdot \nu_2. \tag{2}$$

The complete quantum-mechanical description of neutrino oscillations requires the wave-packet formalism (15). Nevertheless, the correct expressions for the oscillation probabilities can be obtained from Eq. 2 by assuming that the two states have the same momentum or energy (16). The appearance probability to detect ν_e given an initial ν_μ state at a distance L is:

$$P(\nu_\mu \to \nu_e) = \sin^2 2\theta \cdot \sin^2\left(1.27 \cdot \Delta m^2 \cdot \frac{L}{E}\right). \tag{3}$$

Given that the total probability must be conserved, the probability of ν_μ survival or disappearance is simply: $P(\nu_\mu \to \nu_\mu) = 1 - P(\nu_\mu \to \nu_e)$. Here $\Delta m^2 = m_2^2 - m_1^2$ is in units of eV^2, and L/E in km/GeV or m/MeV. In the case of two-neutrino mixing, the same formula applies to oscillations of antineutrinos.

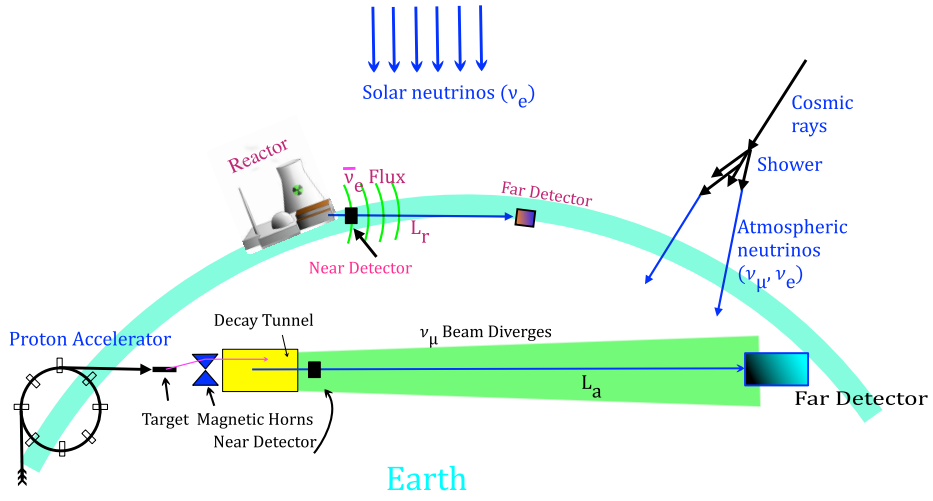

Figure 1: Schematic illustrating neutrino sources that have contributed to the current understanding of neutrino properties through neutrino oscillation experiments. Top: the Sun produces electron neutrinos (ν_e). Right: neutrinos of two types, ν_μ and ν_e, and their antiparticles are produced by collisions of high energy cosmic rays with atoms in the Earth's atmosphere. Middle: nuclear reactors emit electron antineutrinos ($\bar{\nu}_e$) isotropically. Bottom: high energy proton accelerators produce a beam of neutrinos, predominantly ν_μ or $\bar{\nu}_\mu$ that is directed through the Earth.

When traveling through dense matter, neutrino oscillation probabilities can be significantly modified by coherent forward scattering off electrons and nuclei(17, 18). The equation of motion for neutrinos in the simple 2-flavor basis including the effect of matter is written as:

$$i\frac{d}{dt}\begin{pmatrix}\nu_e\\ \nu_\mu\end{pmatrix} = \frac{1}{2}\begin{pmatrix} -(\frac{\Delta m^2}{2E}\cos 2\theta - \sqrt{2}G_F N_e) & \frac{\Delta m^2}{2E}\sin 2\theta \\ \frac{\Delta m^2}{2E}\sin 2\theta & (\frac{\Delta m^2}{2E}\cos 2\theta - \sqrt{2}G_F N_e)\end{pmatrix}\begin{pmatrix}\nu_e\\ \nu_\mu\end{pmatrix}, \tag{4}$$

where G_F is the Fermi constant, N_e is the electron density which could be time (or position) dependent. The product $\sqrt{2}G_F N_e$ acts as an extra potential due to the difference between ν_μ and ν_e scattering amplitude off electrons. This potential reverses sign for antineutrinos. The eigenstates of this system are not the vacuum mass eigenstates ν_1 and ν_2. Under the assumption of constant density a solution in the form of Eq. 3 can be obtained with the following substitutions:

$$\begin{aligned} \sin^2 2\theta &\to \sin^2 2\theta' = \frac{\tan^2 2\theta}{(1-\frac{N_e}{N_e^{res}})^2 + \tan^2 2\theta}, \\ \Delta m^2 &\to \Delta m'^2 = \Delta m^2 \sqrt{(1-\frac{N_e}{N_e^{res}})^2\cos^2 2\theta + \sin^2 2\theta}, \end{aligned} \tag{5}$$

where the quantity

$$N_e^{res} = \frac{\Delta m^2 \cos 2\theta}{2E\sqrt{2}G_F} \approx 6.56\times 10^6 \frac{\Delta m^2[\mathrm{eV}^2]}{E[\mathrm{MeV}]}\cos 2\theta \cdot N_A[\mathrm{cm}^{-3}] \tag{6}$$

is called (for $\Delta m^2 \cos 2\theta > 0$) the resonance density (18, 19) with N_A as Avogadro's number.

Neutrino oscillations take place when the phases of the eigenstates ($E_1 t$ and $E_2 t$) start to differ from each other as a function of time. Over a long period, even extremely small mass differences can lead to sufficient phase difference to cause flavor transformation. Observation of neutrino oscillations implies that neutrinos mix and at least one of them has mass. Neutrinos in the standard model of electroweak interactions are left-handed partners of the charged leptons and only participate in weak interactions. The right-handed components of the neutrino field are absent by definition making neutrinos massless in the model. Consequently, the individual lepton number is strictly conserved as confirmed in rare decays of muons, mesons, and collider experiments (20). Inclusion of neutrino mass in the standard model by simply introducing right-handed partners creates the difficult problem of explaining the smallness and the nature of the neutrino mass as either Dirac or Majorana. Observation of oscillations therefore is considered physics beyond the standard model that not only points to violation of separate lepton number conservation but also forces us to consider that the nature of the neutrino mass (8) could be quite different from the other fermions. On the basis of observed oscillations and limits from direct measurements, the electron neutrino mass is found to be at least five orders of magnitude smaller than the electron, the lightest of the charged fermions (21). But the existing data does not allow determination of neutrinos as Dirac or Majorana fermions.

Experimental Techniques

Figure 1 shows the natural and man-made sources of neutrinos that are the main contributors to our understanding of neutrino oscillations. To be sensitive to oscillations the neutrino energy and the distance to the detector need satisfy the condition $\Delta m^2 \frac{L}{E} \gtrsim 1$ for at least one mass-squared difference. In most cases, moving the detector or the source is impractical to cover a range of L/E, and therefore a broad energy spectrum is beneficial to detect oscillations as a distortion of the expected energy distribution. For solar neutrino experiments ($L \simeq 10^{11}$ m, $E \lesssim 15$ MeV), for atmospheric neutrino experiments ($20 < L < 10000$ km, $E \simeq 1$ GeV), for reactor neutrino experiments ($L \simeq 10 - 100000$ m, $E \simeq 3$ MeV), and for accelerator neutrino experiments ($L \gtrsim 500$ km, $E \simeq 1$ GeV), the sensitivity ranges are $\Delta m^2 \gtrsim 10^{-10}, 10^{-4}, 10^{-5}$, and 10^{-3} eV^2, respectively. In all cases, the event rate per ton of detector is very low because of the small cross section for neutrino interactions, necessitating large detectors. The signal and background characteristics are technique dependent, nevertheless the detectors need to have very good shielding from cosmic ray muons generated in the atmosphere. This can be achieved by placing the detectors deep underground. In the case of accelerator neutrino beams, the pulsed nature of the beam provides additional background suppression.

The Sun is a copious source of ν_e with a flux of $\sim 6 \times 10^{10} \mathrm{cm}^{-2} \mathrm{sec}^{-1}$ at the Earth produced by proton-proton and carbon-nitrogen-oxygen fusion reactions (22). The solar ν_e spectrum is calculated using the standard solar model (SSM) with uncertainties ranging from <1% for the $pp \rightarrow de^+\nu$ component to ~14% for the higher energy Boron-8 component ($\lesssim 15$ MeV). Solar neutrinos are detected using charged-current neutrino reactions on nuclei with low thresholds or using elastic scattering from electrons. In the presence of oscillations, a depletion of the expected ν_e flux is observed.

Nuclear fission reactors produce electron antineutrinos generating $\sim 2 \times 10^{20}$ $\bar{\nu}_e$

per GW of thermal power. As products of decay chains of neutron rich nuclei, these $\bar{\nu}_e$ are emitted isotropically from the core with an energy spectrum predominantly below 8 MeV (23,24). They are detected via the inverse beta decay (IBD) reaction, $\bar{\nu}_e + p \rightarrow e^+ + n$, in detectors that contain free protons. The energy of an incoming antineutrino is determined by measuring the positron energy, while the detection of the recoiling neutron, in coincidence with the positron signal, suppresses backgrounds.

Atmospheric neutrinos have an approximately isotropic flux of $\sim 4000\ \mathrm{m}^{-2}\mathrm{sec}^{-1}$ on the Earth from the decay of π and K mesons produced in interactions of cosmic rays in the upper atmosphere. The dominant contributions come from the decay chains, $\pi^{\pm} \rightarrow \mu^{\pm} + \nu_{\mu}(\bar{\nu}_{\mu})$ and $\mu^{\pm} \rightarrow e^{\pm} + \nu_e(\bar{\nu}_e) + \nu_{\mu}(\bar{\nu}_{\mu})$. The flux has a falling energy spectrum with a peak ~ 1 GeV, and flux ratio $\Phi(\nu_{\mu} + \bar{\nu}_{\mu})/\Phi(\nu_e + \bar{\nu}_e) \approx 2$ (25,26). Charged-current interactions of atmospheric neutrinos in large underground detectors allow study of oscillations over large distances (~ 10 km from above to 1.3×10^4 km from below) using the well-understood flux which must be up-down symmetric (within $\lesssim 0.5\%$) in the absence of oscillations (27).

Accelerator neutrino beams are produced by bombarding high energy protons into a stationary target. The emerging π and K mesons are collected by a system of magnetic lenses (horns) (28), collimated towards the detector, and allowed to decay within a shielded tunnel into muons and neutrinos. The neutrino energy can be in the range of $\lesssim 0.5$ GeV to $\gtrsim 100$ GeV. The flux can be sign-selected to be predominantly ν_{μ} or $\bar{\nu}_{\mu}$ with a small contamination ($\sim 1\%$) from electron type. The primary proton energy, the geometry of the target, horns, as well as the horn current can be adjusted to tune the beam spectrum with great flexibility.

An important aspect of reactor and accelerator experiments is the ability to place near and far detectors to study the same source. The near detector is placed sufficiently close to the source to measure the neutrino flux before any significant flavor transformation. The far detector can be positioned in the location of the expected oscillation maximum to measure the spectrum and flavor composition after oscillations. The comparison of observations at the two sites allows for accurate determinations of oscillation parameters free of many uncertainties associated with neutrino production and interaction rates.

In Sec. 2, we review the 3-flavor neutrino model and summarize the experimental progress over the past several decades in establishing it. In Sec. 4 and Sec. 5, we examine the current and future planned long-baseline experiments which aim to determine the remaining unknowns and improve the precision of known neutrino parameters. We will describe the motivation for a program of long-baseline neutrino experiments with particular emphasis on determination of the neutrino mass ordering and search for new charge-parity (CP) symmetry violation.

Although the discovery of neutrino oscillations took place using natural sources of neutrinos from the Sun and the atmosphere, future precise measurements are expected to originate from man-made sources such as reactors and accelerators that are well-monitored and controllable. As described in Sec. 5, future measurements of CP violation will only be possible in a long-baseline accelerator-based, high-power, and pure neutrino beam directed at a near detector and a very large and capable far detector.

2 The Three-flavor neutrino Standard Model

Although a definitive description of massive neutrinos within the standard model does not yet exist, all compelling neutrino oscillation data can be described by mixing among three left-handed neutrino flavors, ν_e, ν_μ, ν_τ in analogy with quark mixing via the Cabibbo-Kobayshi-Maskawa (CKM) matrix (7). This number of active neutrinos is also compatible with the measured invisible decay width of the Z-boson. The data firmly establishes that the 3 neutrino flavors are superpositions of at least 3 light mass states with unequal masses, $m_1 \neq m_2 \neq m_3$, all smaller than ~ 1 eV. The oscillations are characterized by two independent mass differences: $\Delta m^2_{21} = m^2_2 - m^2_1$ and $\Delta m^2_{32} = m^2_3 - m^2_2$ with $\Delta m^2_{31} = \Delta m^2_{32} + \Delta m^2_{21}$. The unitary 3×3 mixing matrix, U, called the Pontecorvo-Maki-Nakagawa-Sakata (PMNS) matrix, is parameterized by 3 Euler angles and depending on whether the ν_j are Dirac or Majorana, 1 or 3 phases potentially leading to CP violation.

$$\nu_{lL} = \sum_{j=1}^{3} U_{lj}\nu_{jL} \tag{7}$$

$$U = \begin{pmatrix} c_{13}c_{12} & c_{13}s_{12} & s_{13}e^{-i\delta_{CP}} \\ -c_{23}s_{12} - s_{13}s_{23}c_{12}e^{i\delta_{CP}} & c_{23}c_{12} - s_{13}s_{23}s_{12}e^{i\delta_{CP}} & c_{13}s_{23} \\ s_{23}s_{12} - s_{13}c_{23}c_{12}e^{i\delta_{CP}} & -s_{23}c_{12} - s_{13}c_{23}s_{12}e^{i\delta_{CP}} & c_{13}c_{23} \end{pmatrix} \times diag(1, e^{i\frac{\alpha_{21}}{2}}, e^{i\frac{\alpha_{31}}{2}}) \tag{8}$$

Here, $c_{ij} = \cos\theta_{ij}$ and $s_{ij} = \sin\theta_{ij}$, δ_{CP} is the Dirac phase, and α_{21} and α_{31} are Majorana phases that cannot be observed in oscillation experiments. Including the 3 neutrino masses there are a total of 7 or 9 additional free parameters in the minimally extended standard model with massive neutrinos for the cases of Dirac or Majorana neutrinos, respectively. The full oscillation phenomenology is then described by modifying Eq. (3) for 3-ν mixing. For neutrinos produced with energy E and flavor l, the probability of its transformation to flavor l' after traveling a distance L in vacuum is expressed as:

$$\begin{aligned} P_{ll'} \equiv P(\nu_l \to \nu_{l'}) &= \left| \sum_i U_{li} U^*_{l'i} e^{-i(m^2_i/2E)L} \right|^2 \\ &= \sum_i |U_{li}U^*_{l'i}|^2 + \Re \sum_i \sum_{j\neq i} U_{li}U^*_{l'i}U^*_{lj}U_{l'j} e^{i\frac{\Delta m^2_{ij}L}{2E}}. \end{aligned} \tag{9}$$

The best values for the parameters can be obtained from a global fit to the data of neutrino oscillation experiments (7,29) The measured mass-squared differences are $\Delta m^2_{21} \approx 7.5 \times 10^{-5}$ eV^2, $|\Delta m^2_{32}| \approx 2.4 \times 10^{-3}$ eV^2, where the sign of Δm^2_{32} is unknown and is commonly referred to as the problem of mass ordering or hierarchy (MH). The determined mixing angles are $\theta_{12} \cong 33.5^\circ$, $\theta_{13} \cong 8.4^\circ$, and $\theta_{23} - 45^\circ \sim 3^\circ$ for normal and $\theta_{23} - 45^\circ \sim -4.5^\circ$ for inverted mass ordering. Currently θ_{23} is the least known mixing angle with a strong degeneracy around $\pi/4$ because the measurement is dominated by disappearance of ν_μ which measures $\sin^2 2\theta_{23}$. From global fits (29, 30) to the data the current 1 σ uncertainties on the parameters Δm^2_{21}, $\sin^2\theta_{12}$, $|\Delta m^2_{32}|$, $\sin^2\theta_{23}$, and $\sin^2\theta_{13}$ are about 3%, 4%, 2%, 12%, and 5%, respectively. Finally, the current experimental data does not significantly constrain the Dirac CP phase.

Since the ratio of the two mass differences, $\Delta m^2_{32}/\Delta m^2_{21} \cong 33$, is large, most experimental situations can be analyzed using a 2-ν model with small corrections. If the experimental situation is such that $\Delta m^2_{21} L/(2E) \sim 1$ and $|\Delta m^2_{31}| L/(2E) \gg 1$ then oscillations due to the larger Δm^2 are averaged out due to either the size of the production region or experimental energy resolution. On the other hand, if $|\Delta m^2_{31}| L/(2E) \sim 1$ then the oscillations due to the smaller Δm^2_{21} remain a small correction. Fig. 2 illustrates the distinctive pattern of masses and mixings in the neutrino sector. The normal or NH (inverted or IH) mass ordering is on the left (right). The maximal ν_μ/ν_τ mixing in ν_3 is parameterized by θ_{23}. The potentially large CP asymmetry is demonstrated as a variation of flavor content within each mass state.

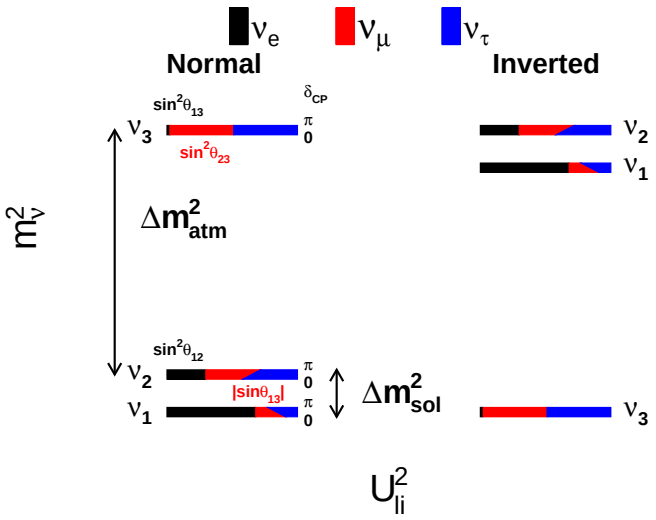

Figure 2: Patterns of the neutrino masses and mixing for normal (left) and inverted (right) ordering (31).

2.1 Measurement of $|\Delta m^2_{32}|$ and θ_{23}

The first compelling evidence of neutrino flavor oscillation was obtained by the Super-Kamiokande (Super-K) experiment observing atmospheric neutrinos. The cylindrical Super-K detector contains 50 ktons of pure water 1000 m underground in western Japan. Charged particles with velocities exceeding that of light in water emit Cherenkov radiation which is detected using regularly spaced large photo-multiplier tubes along the walls, sensitive to single photo-electrons (32). For atmospheric neutrinos, the detection principle relies on observing Cherenkov light from the charged lepton produced in the reaction: $\nu_l + N \to l + N'$. The energy, direction, and flavor of the incoming neutrino is reconstructed from the detected pattern, arrival times, and intensity of Cherenkov photons.

In 1998 Super-K reported a zenith angle dependent deficit of the upward going atmospheric muon neutrinos, inconsistent with the expected nearly isotropic flux (33). This definitive result followed the earlier hints from previous water Cherenkov detectors, Kamioka Nucleon Decay Experiment (KamiokaNDE) and Irvine-Michigan-Brookhaven (IMB) (34, 35). The deficit of upward going muon neutrinos was not accompanied by excess of upward going electron neutrinos. This indicated that ν_μ were oscillating into ν_τ which could not be observed in the

detector due to the high energy threshold ($\sim$3.5 GeV) required for τ production and the extremely short τ lifetime.

The discovery of atmospheric neutrino oscillations was possible because of the large available dynamic range in L/E, the necessary event statistics provided by the massive underground detectors, and the favorably large θ_{23} mixing (36). Super-K obtains the best precision on the $\nu_\mu \rightarrow \nu_\mu$ parameters through selection of muon type events with good energy and angular resolution to prepare an analysis using L/E as the observable. As demonstrated in (37) the event depletion at $\sim$ 500 km/GeV corresponds to the first oscillation maximum with $|\Delta m^2| \approx (\pi/2) \times (1/500)$ eV^2. At $L/E \gg 500$ km/GeV, the fast oscillations cannot be resolved, and an average factor of 1/2 depletion of ν_μ type events is measured corresponding to a precise measurement of $1-\frac{1}{2}\sin^2 2\theta$ or near-maximal mixing. In the 3-neutrino scenario Super-K measures $|\Delta m^2_{32}|$ (the atmospheric mass-squared splitting) and a product of matrix elements $4|U_{\mu 3}|^2\cdot(|U_{\mu 1}|^2+|U_{\mu 2}|^2)$. The latter further converts to a measurement of θ_{23} (the atmospheric mixing angle).

The unusually large neutrino mixing observed in the atmospheric oscillations discovery needed a confirmation by accelerator neutrino experiments in which the neutrino beam is tunable and has high purity. Independent confirmation came from K2K (KEK to Kamioka) (38), MINOS(Main Injector Neutrino Oscillations) (39), and T2K (Tokai to Kamioka) (40) in which disappearance of muon neutrinos was observed with a laboratory produced beam. The most precise measurements of $|\Delta m^2_{32}|$ and θ_{23} are currently obtained by MINOS (41) and T2K (42), respectively. Figure 3 shows the muon neutrino spectrum observed in MINOS. MINOS uses an accelerator produced beam from the Fermilab (USA) Main Injector accelerator with 120 GeV protons; the peak energy of the low energy neutrino beam is adjusted to be about 3 GeV. The MINOS far detector is a magnetized steel scintillator detector with 5 ktons of mass located 735 km away in the Soudan mine; in addition MINOS has a near detector using the same technology with 1 kton of mass placed $\sim$1 km away from the beam production target. A unique feature of MINOS is the ability to run the beam with changes to the target position and the horn current. By fitting several different spectra in the near detector, MINOS is able to make predictions with $\lesssim 4\%$ uncertainty (43) for the far detector event spectrum without oscillations which is important for parameter determination.

T2K uses an accelerator produced beam from the JPARC (Japan Proton Accelerator Research Complex) accelerator with 30 GeV protons; the Super-K water Cherenkov detector is used as the far detector located 295 km away. The direction of the beam is adjusted to be off-axis (44) by 2.5^o to obtain a narrow band beam with maximum at 0.6 GeV (45) and width of $\sim$ 0.3 GeV. The Super-K water Cherenkov detector has excellent energy and particle identification capability at this energy allowing the experiment to see almost complete disappearance of muon neutrino events at $L/E \sim 295/0.6$ km/GeV. The off-axis technique with excellent energy resolution could provide the best determination of $\sin^2 2\theta_{23}$.

In addition to confirming the ν_μ disappearance signal, it was important to explicitly test for $\nu_\mu \rightarrow \nu_\tau$ as indicated by the atmospheric neutrino result. Such a test requires detection of τ leptons from a charged current interaction of ν_τ at high energies. As the τ lepton decays almost immediately ($c \cdot \tau_{lifetime} \sim 87$ μ m), even a boosted τ with a momentum of $\sim$2 GeV/c would only travel about tenth of a mm before decay. Furthermore, the τ decays to a variety of final

states making it difficult to distinguish from neutral current events. Despite these difficulties Super-K collaboration has statistically identified ν_τ events at 3.8σ in the atmospheric neutrino data from the backgrounds generated by deep inelastic scattering of ν_μ and ν_e (46). Detection of individual ν_τ events requires tracking and detection of τ decays at very short distances. The direct observation of ν_τ appearance in a ν_μ beam was performed by the OPERA (Oscillation Project with Emulsion Tracking) experiment using emulsion films with spatial resolution of ~ 1 μm (47). OPERA has reported observation of 5 τ events with an expected background of 0.25 events confirming the dominance of the $\nu_\mu \rightarrow \nu_\tau$ oscillation mode (48, 49).

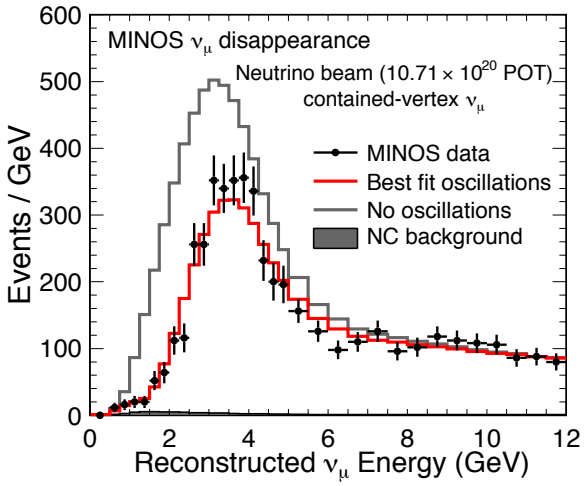

Figure 3: Distribution of muon neutrino events plotted as a function of reconstructed energy in the MINOS far detector (50) at a distance of 735 km. The solid grey line shows the expected spectrum under no oscillation hypothesis. The depletion of events at $\gtrsim$ 1.5 GeV and the shape of the depleted spectrum is consistent with dominant $\nu_\mu \rightarrow \nu_\tau$ oscillations with maximal mixing.

2.2 Measurement of Δm^2_{21} and θ_{12}

Starting in 1967, Ray Davis measured the solar ν_e flux with 610 tons of liquid C_2Cl_4 through the reaction $\nu_e + {}^{37}\mathrm{Cl} \rightarrow e^- + {}^{37}\mathrm{Ar}$. The solar neutrino rate was determined by periodically counting decays of radioactive ^{37}Ar extracted from the detector liquid. The measured ν_e flux was only about 1/3 (51) of the prediction from the standard solar model (SSM) (52). This result was further confirmed by the Gallium experiments, SAGE (53) and GALLEX (54), using the $\nu_e + {}^{71}\mathrm{Ga} \rightarrow {}^{71}\mathrm{Ge} + e^-$ reaction as well as Kamiokande (55) and Super-K (56, 57) experiments using the $\nu_e + e^- \rightarrow \nu_e + e^-$ reaction. Neutrino mixing offered a natural explanation to the solar neutrino puzzle, since the some of ν_e generated in the Sun could transform to muon or tau neutrino flavors during flight and thus become undetectable due to the low solar neutrino energies which are below the thresholds for muon and tau production.

The Sudbury Neutrino Observatory (SNO) experiment was designed to measure the flux of all neutrino flavors from the Sun using the neutral current reaction on deuterium, $\nu + d \rightarrow \nu + p + n$, and separately the ν_e flux through the charged-

current reaction $\nu_e + d \rightarrow e^- + p + p$. SNO was a water Cherenkov detector with an active target mass composed of $\sim$ 1 kton of heavy water (D_2O) which provides the deuterium targets for solar neutrinos. The final-state neutron from the neutral-current reaction was detected by a variety of techniques with consistent results. Measurement of the electron energy from the final state of the charged current reaction determines the solar neutrino spectrum above $\sim$ 5 MeV (58). The results (59) are consistent with the predictions of SSM incorporating ν-oscillations enhanced by the matter effect in the Sun. Borexino in Italy is an extremely high resolution liquid scintillation underground detector and has contributed by measuring the elastic scattering reaction, $\nu + e \rightarrow \nu + e$, for ν_e energies below the ^{7}Be line (0.861 MeV) in the solar neutrino spectrum. The solar ν_e survival probability as function of energy is obtained by combining data collected at all energies using the radiochemical experiments, Borexino, SNO, and Super-K (60).

The electron density in the core of the Sun is $N_e \sim 100\ N_A \mathrm{cm}^{-3}$ and it drops approximately exponentially to 0 at the surface. An electron neutrino of energy $\lesssim$ 1 MeV generated in the core of the Sun has a resonance density N_e^{res} much larger than N_e and therefore according to Eq. (5) the oscillations are as if in vacuum. The spread due to distance and the source size wash out the oscillations and the survival probability is a constant $\sim 1 - \frac{1}{2}\sin^2 2\theta_{12}$. At energy $\gtrsim$ 5 MeV, $N_e^{res} < N_e$ and the ν_e eigenstate inside the Sun coincides with the heavier effective mass eigenstate which adiabatically evolves into ν_2 as the density decreases. In this energy region the ν_e produced in the core leave the Sun in the ν_2 state with the ν_e survival probability $\sim \sin^2\theta_{12}$. This effect is called the Mikheyev-Smirnov-Wolfenstein (MSW) effect (17,61–63). The energy dependent survival probability additionally provides the constraint $\Delta m^2_{21} \cdot \cos 2\theta_{12} > 0$ and is a confirmation of the matter effect. In the 3-ν picture, the charge current (ν_e only) and the neutral current (sum of all ν_l) solar rate is a constraint on a combination of the PMNS matrix elements $|U_{e2}|^2 \cdot (|U_{e1}|^2 + |U_{e2}|^2) + |U_{e3}|^4$ or $\cos^4\theta_{13}\sin^2\theta_{12} + \sin^4\theta_{13}$.

The Sun is a broadband source of pure ν_e, and when combined with the enhancement due to the MSW effect and the very long distance to the Earth, it is not surprising that solar neutrino experiments provided the first hint of neutrino oscillations. Nevertheless, despite consistency with the large mixing angle θ_{12}, no neutrino experiment can exclude the possibility of multiple solutions with sufficient statistical significance. The Kamioka liquid-scintillator antineutrino detector (KamLAND) experiment (64) in Japan resolved this ambiguity with detection of reactor $\bar{\nu}_e$ over a long distance. There are a large number of nuclear power reactors around the KamLAND site with a flux averaged distance of $\sim$180 km. With neutrino energy determined from the measured positron energy in the IBD process, KamLAND was able to observe the L/E oscillation spectrum shown in Fig. 4. Taking advantage of the very different L/E ranges of the atmospheric and reactor neutrinos, KamLAND and the solar neutrino experiments can be understood in the 2-ν framework and provide $\Delta m^2_{21} \sim 7.5 \times 10^{-5}$ eV^2 (the solar mass-squared splitting) and $\theta_{12} \sim 34^\circ$ (the solar mixing angle). Within the 3-ν framework the KamLAND $\bar{\nu}_e$ disappearance constrains Δm^2_{21} and a combination of PMNS matrix elements $2|U_{e3}|^2 \cdot (|U_{e1}|^2 + |U_{e2}|^2) + 4|U_{e1}|^2 \cdot |U_{e2}|^2$. The latter is mostly sensitive to the solar mixing angle θ_{12} and has a weak dependence on the mixing angle θ_{13}.

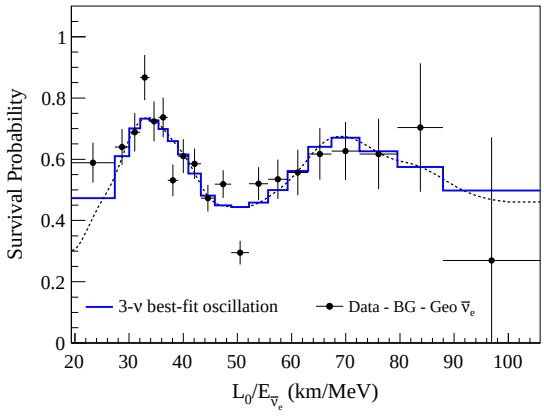

Figure 4: Survival probability of $\bar{\nu}_e$ events as a function of L/E in the KamLAND far detector (65). The dip position of the oscillation ($\sim$50 km/MeV) is consistent with the second oscillation node for Δm^2_{21}. The size of the depletion is a measurement of $\sin^2 2\theta_{12}$.

2.3 Measurement of θ_{13}

The key observation to complete the 3-ν picture is the determination of ν_e oscillations in the same L/E range as indicated by the atmospheric Δm^2_{32}. The main impact of this observation is an explicit demonstration that the ν_e state is composed of three mass eigenstates or that all elements in the top row of the matrix in Eq. (8) are non-zero. Both the solar and KamLAND measurements have a weak dependence on θ_{13}. A joint analysis of these data provided an initial hint for a non-zero value (66). Previous reactor experiments with baseline of $\sim$ 1 km (67–69) and a single far detector provided upper limits $\sin^2 2\theta_{13} \lesssim 0.12$ at 90% C.L..

A new campaign of experiments was launched to determine θ_{13} by either $\bar{\nu}_e$ disappearance with reactors or $\nu_\mu \to \nu_e$ ($\bar{\nu}_\mu \to \bar{\nu}_e$) appearance with accelerators. In the case of reactor experiments, the maximum expected depletion was $\lesssim 10\%$, and so a carefully designed experiment with near and far detectors was needed. In the case of accelerators, the ν_e signal was expected to have low statistics with background from both neutral current events and the ν_e contamination in the ν_μ beam, and therefore a well-designed neutrino beam and a large detector with excellent electron identification were needed.

In 2012, three new reactor experiments reported results on θ_{13}. Double Chooz (France) reported results with a far detector only (70) disfavoring $\theta_{13} = 0$ at 1.6σ. The Daya Bay experiment (China) reported the discovery of non-zero θ_{13} with $\gtrsim 5\sigma$ significance from an array of three near, and three far identical detectors (each with 20 tons of gadolium-loaded liquid scintillator fiducial mass) placed to optimize sensitivity from three nuclear power stations (71). RENO (Reactor Experiment for Neutrino Oscillations) also reported results from an array of nuclear power stations in Korea and identical near and far Gd-loaded liquid scintillator detectors confirming Daya Bay's discovery with a 4.9σ significance (72). Daya Bay increased their significance to $>10\sigma$ with a larger data set (73) and recently

added more target mass to the far and near sites (4 near and 4 far detectors) (74). The additional statistics and careful energy calibration in Daya Bay has resulted in an independent measurement of Δm^2_{31} which governs this oscillation (Fig. 5). The third neutrino mixing angle θ_{13} is now precisely measured to be $\sim$8.4°. MINOS (75) and T2K (76) have reported their searches of ν_μ to ν_e oscillation that is also sensitive to θ_{13}. In particular, T2K obtained an early result disfavoring $\theta_{13} = 0$ at 2.5σ. The status of current accelerator experiments addressing $\nu_\mu \to \nu_e$ will be covered in more detail in the next section.

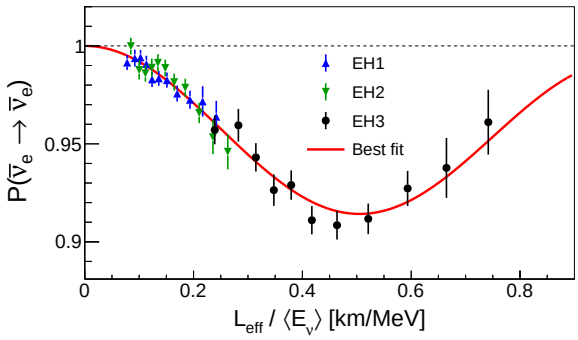

Figure 5: The measured $\bar{\nu}_e$ disappearance probability is shown as a function of of L/E from Daya Bay (74). The associated oscillation frequency corresponds to $\Delta m^2_{31} \sim \Delta m^2_{32} \sim 2.4 \times 10^{-3}$ eV^2.

The picture of masses and mixings illustrated in Fig. 2 was assembled over several decades, mainly using precise observations of ν_μ or ν_e disappearance. By convention $m_2 > m_1$, and the strong evidence of matter effect in the Sun indicates $\Delta m^2_{21} \cos 2\theta_{12} > 0$ leading to $\theta_{12} < \pi/4$. But the question of neutrino mass hierarchy, whether ν_3 is heavier or lighter than $\nu_{1,2}$, remains unresolved (77). The sign of $\theta_{23} - \pi/4$ and the Dirac or Majorana phases are also unknown. These questions as well as further precision measurements are expected to be addressed by running and future experiments optimized for the known parameters and focused on appearance measurements of $\nu_\mu \to \nu_e$ conversion.

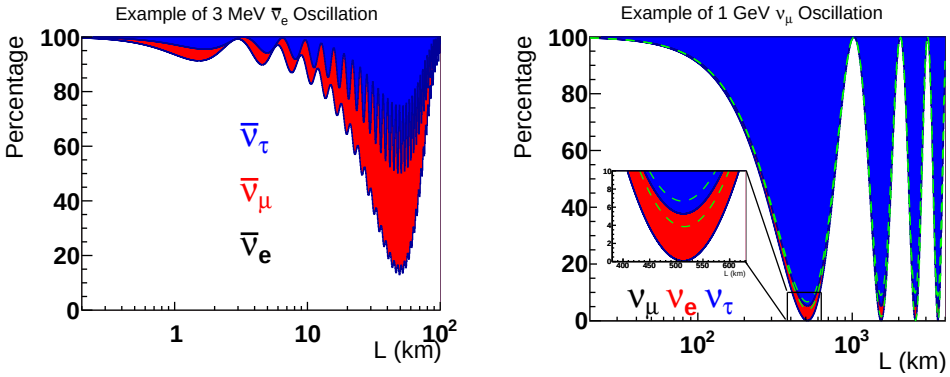

Figure 6: Examples of neutrino oscillations in matter using the 3-neutrino oscillation model. This calculation assumes $m_3 > m_2 > m_1$. The left hand plot displays the evolution of a 3 MeV electron antineutrino. The right hand plot displays the evolution of a 1 GeV muon type neutrino.

The precise prediction of 3 neutrino oscillations using the PMNS matrix model in matter is shown in Fig. 6. For the left panel, the flavor evolution of a 3 MeV electron antineutrino – typical of a reactor experiment – is shown over a distance of 100 km. Due to the large difference between Δm^2_{21} and $|\Delta m^2_{32}|$, two different oscillation frequencies are seen with a relative shift dependent on the sign of Δm^2_{32}. Reactor experiments can only observe $\bar{\nu}_e$ disappearance as the neutrino energies are too low for muon and tau production in charged-current reactions.

For the right panel in Fig. 6, the flavor evolution of a 1 GeV muon neutrino – typical of an accelerator experiment – is shown over a distance 5000 km. According to the best fit parameters such neutrinos should undergo a complete transformation after about ∼500 km with a small fraction appearing as ν_e. The ν_e fraction undergoes a large modulation depending on the unknown CP phase (dashed lines represent $\delta_{CP} = \pm\pi/2$), and is opposite in magnitude for neutrinos and antineutrinos. The CP effect also grows for higher oscillation nodes. A properly designed experimental program using reactor and accelerator sources should allow us to measure these oscillations over several nodes, to uncover if a large CP violation exists in the lepton sector, and to precisely determine the parameters including the mass hierarchy and the possibility of maximum mixing.

A few anomalous experimental results including LSND (78), MiniBooNE (79), and measurements of absolute reactor flux (80) cannot be explained by the 3-neutrino framework. These results suggest that the 3×3 PMNS matrix might not be unitary, and there might exist sterile neutrino(s) with the mass-squared splitting $\Delta m^2_{41} \sim 1$ eV$^2 \gg |\Delta m^2_{32}| \sim |\Delta m^2_{31}| \gg \Delta m^2_{21}$ with small mixing with the three active neutrinos. Details about these data and future direct searches at short baselines ($L/E \sim 1$ km/GeV) can be found in Ref. (81). A joint fit of the current solar, KamLAND, and Daya Bay results provides the first unitarity test of the top row of the PMNS matrix ($|U_{e1}|^2 + |U_{e2}|^2 + |U_{e3}|^2 - 1 \approx \pm 0.04$), insufficient to exclude sterile neutrinos with small mixing. (82, 83). The comparison of θ_{13} derived from reactor disappearance measurements and from accelerator appearance measurements also provides a strong indirect test of the unitarity of PMNS matrix (83). In the rest of this review, we will focus on the standard three-flavor neutrino model and precise measurements of its parameters with current and future long-baseline experiments.

3 Phenomenology of CP violation and mass hierarchy

We first examine the appearance probability $P_{\mu e}$ in the 3-flavor model to understand the experimental optimization:

$$P_{\mu e} = |U_{\mu 1} U^*_{e_1} e^{-iE_1 t} + U_{\mu 2} U^*_{e_2} e^{-iE_2 t} + U_{\mu 3} U^*_{e_3} e^{-iE_3 t}|^2 \qquad (10)$$

where $E_i t$ represents the phase advance of the mass eigenstate ν_i over the flight time between the source and the detector. The oscillation probability for $\nu_e \to \nu_\mu$ or $\bar{\nu}_\mu \to \bar{\nu}_e$ can be obtained by simply exchanging the labels $(e) \leftrightarrow (\mu)$. Therefore, if any element of the PMNS matrix is complex, (e.g. $U_{e3} \neq U^*_{e3}$), neutrino oscillations are not invariant under time reversal or charge-parity conjugation. This is a phenomenological consequence of 3-generation mixing with at least one complex phase.

Explicitly, if the PMNS matrix is complex, then the asymmetry $a^{ll'}_{CP} \equiv P(\nu_l \to \nu_{l'}) - P(\bar{\nu}_l \to \bar{\nu}_{l'})$ is a direct measurement of the CP violation in the neutrino system. In the case of 3-neutrino mixing, $a^{\mu e}_{CP} = -a^{\tau e}_{CP} = a^{\tau\mu}_{CP}$. We

prefer to use the fractional asymmetry in experimental considerations: $A^{ll'} \equiv (P(\nu_l \to \nu_{l'}) - P(\bar{\nu}_l \to \bar{\nu}_{l'}))/(P(\nu_l \to \nu_{l'}) + P(\bar{\nu}_l \to \bar{\nu}_{l'}))$. The preferred observable is $A^{\mu e}$ since it is expected to be large, and the production and detection of ν_μ and ν_e is far easier than ν_τ. For vacuum oscillations the CP asymmetry to leading order in $\alpha = \Delta m^2_{21}/\Delta m^2_{31}$ is:

$$A^{\mu e}_{CP} \approx \frac{2J^{PMNS}_{CP}}{\sin^2(\theta_{23})\sin^2(\theta_{13})\cos^2(\theta_{13})} \times \alpha \frac{\Delta m^2_{31} L}{4E_\nu}, \tag{11}$$

where J^{PMNS}_{CP} is the rephasing invariant (7),

$$J^{PMNS}_{CP} \equiv \frac{1}{8}\sin 2\theta_{12}\sin 2\theta_{13}\sin 2\theta_{23}\cos\theta_{13}\sin\delta_{CP} \approx 0.032\sin\delta_{CP}. \tag{12}$$

This is in sharp contrast to the very small mixing in the quark sector which leads to the very small value for the corresponding invariant: $J^{CKM}_{CP} \approx 3 \times 10^{-5}$, despite the large value of $\delta^{CKM}_{CP} \sim 70^o$. Recent studies in leptogenesis (84) have shown that the phases in the PMNS matrix can provide the CP violation large enough for the generation of observed baryon asymmetry of the universe (85,86). Therefore observation of CP violation due to J^{PMNS}_{CP} could account for a large fraction of the baryon asymmetry (87, 88). The asymmetry $A^{\mu e}_{CP}$ increases as a function of L/E and is shown to decrease with $\sin\theta_{13}$ (89, 90) as long as it is not too small, and with current parameters the asymmetry can be as large as $\sim 32\%$ for $L/E \sim 500$ km/GeV (91). Due to the linear dependence on L, and $\sin\theta_{13}$, the statistical error on $A^{\mu e}_{CP}$ is approximately independent of L and θ_{13} providing substantial flexibility in experimental considerations (89, 92).

Observation of $A^{\mu e}_{CP}$ requires a long-baseline experiment with a pure accelerator generated beam of ν_μ and $\bar{\nu}_\mu$ crossing the Earth before reaching the detector. The effect of Earth matter must be taken into account using the electron density through the crust or mantle of $N_e \cong 1.8 N_A$ cm^{-3}. Using the well-known values of $|\Delta m^2_{32}|$ and θ_{13}, for typical accelerator neutrino energy of $\sim 1 - 10$ GeV large change is expected to the oscillation probability (Eq. (4) and (6)). The effect for neutrinos (anti-neutrinos) leads to an enhancement (suppression) for $m_3 > m_2 > m_1$ and a suppression (enhancement) for $m_1 < m_2 < m_3$, and therefore measuring it will determine the order of the neutrino masses. Atmospheric neutrinos are also expected to show significant sensitivity to Earth matter for $E_\nu > 2$ GeV crossing the core (93,94). The effect of Earth matter on neutrino oscillations with accelerator or atmospheric neutrinos has not been demonstrated in a definitive way, therefore such a measurement has interest both for phenomenology and for determining the mass ordering.

Since the size of the effect on $P_{\mu e}$ due to the CP phase and the Earth matter is similar, both effects have to be considered for actual experiments. For accelerator experiments, assuming a constant density of matter, a sufficiently accurate expression to leading order in $\alpha = \Delta m^2_{21}/\Delta m^2_{31}$ has been derived (95)(also see

Fig. 6):

$$
\begin{aligned}
P(\nu_\mu \to \nu_e) &= \sin^2\theta_{23}\frac{\sin^2 2\theta_{13}}{(A-1)^2}\sin^2[(A-1)\Delta_{31}] \\
&+ \alpha^2\cos^2\theta_{23}\frac{\sin^2 2\theta_{12}}{A^2}\sin^2(A\Delta_{31}) \\
&- \alpha\frac{\sin 2\theta_{12}\sin 2\theta_{13}\sin 2\theta_{23}\cos\theta_{13}\sin\delta_{CP}}{A(1-A)}\sin\Delta_{31}\sin(A\Delta_{31})\sin[(1-A)\Delta_{31}] \\
&+ \alpha\frac{\sin 2\theta_{12}\sin 2\theta_{13}\sin 2\theta_{23}\cos\theta_{13}\cos\delta_{CP}}{A(1-A)}\cos\Delta_{31}\sin(A\Delta_{31})\sin[(1-A)\Delta_{31}],
\end{aligned}
\tag{13}
$$

where

$$\Delta_{ij} = \Delta m^2_{ij} L/4E_\nu,\ A = \sqrt{2}G_F N_e 2E_\nu/\Delta m^2_{31}.$$

For anti-neutrinos the signs of δ_{CP} and A are reversed. The last two terms in the expression are proportional to J^{PMNS}_{CP}. The dependence on the mass hierarchy in A and the CP phase can be disentangled with precise measurement of $\nu_\mu \to \nu_e$ and $\bar{\nu}_\mu \to \bar{\nu}_e$ appearance as a function of energy (92, 96).

The precise measurement of $\sin^2 2\theta_{13}$ by reactor neutrino experiments (97, 98) has also provided a unique opportunity to determine the neutrino mass hierarchy in a medium-baseline high resolution reactor neutrino oscillation experiment (99–110). The energy and distance for reactor experiments is sufficiently low that the vacuum formula for the survival probability of an electron antineutrino can be used (see Fig. 6):

$$
\begin{aligned}
P(\nu_e \to \nu_e) &= 1 \\
&- \cos^4(\theta_{13})\sin^2(2\theta_{12})\sin^2(\Delta_{21}) \\
&- \cos^2(\theta_{12})\sin^2(2\theta_{13})\sin^2(\Delta_{31}) \\
&- \sin^2(\theta_{12})\sin^2(2\theta_{13})\sin^2(\Delta_{32}),
\end{aligned}
\tag{14}
$$

This depends on mass hierarchy as $|\Delta_{31}| > |\Delta_{32}|$ for NH and $|\Delta_{31}| < |\Delta_{32}|$ for IH. The measured reactor neutrino energy spectrum for $\Delta m^2_{21} L/(2E) \sim 1$ (or $L \sim 50$km) is expected to exhibit oscillations with a slow (Δ_{21}) and a fast component. The fast component due to ($\Delta_{31} \approx \Delta_{32}$) has amplitude proportional to $\sin^2(2\theta_{13})$. The two choices for mass hierarchy produce a small energy dependent shift (of the order of $\Delta m^2_{21}/\Delta m^2_{32} \sim \pm 3\%$) in the oscillation pattern which can be measured with sufficient energy resolution. From above formula, well-optimized reactor experiments can access five neutrino mixing parameters: θ_{12}, Δm^2_{21}, θ_{13}, $|\Delta m^2_{32}|$, and the mass hierarchy (or the sign of Δm^2_{32}). Such high precision measurements will enable tests of neutrino mass and mixing models. For example, models of quark-lepton complementarity and others (111, 112), have predicted $\theta_{12} + \theta_{Cabbibo} = \pi/2$ and $\theta_{13} \approx \theta_{Cabbibo}/\sqrt{2}$.

Based on Eq. (13) and Eq. (14), an optimized program of measurements for appearance for $\nu_\mu \to \nu_e$ using an accelerator ν_μ beam, and disappearance for $\bar{\nu}_e \to \bar{\nu}_e$ using reactor flux cover the remaining issues within neutrino oscillation physics. They also provide redundancy for measurements of mass hierarchy, Δm^2_{32}, and θ_{13}. These measurements depend on man-made pure beam sources with optimized L/E range. Neutrino physics phenomenology has proven to be quite rich and any future program should not only be guided by measurements motivated by the current best model, but should also be sufficiently redundant

and with enough dynamic range to allow identification of new physics effects if they exist. In the next sections we will examine the current and future planned programs for these measurements.

4 Current-generation of Experiments

The accelerator disappearance experiment MINOS+ (113), and the reactor experiments Daya Bay, Double Chooz, and RENO are expected to continue operations to improve precision on Δm^2_{32}, $\sin^2 2\theta_{23}$ and $\sin^2 2\theta_{13}$. The error on the value of the $\sin^2\theta_{13}$ is expected to reach $\sim$3% (114). The sign and magnitude of $\theta_{23} - \pi/4$ is of significance for the theoretical work aimed at explaining underlying symmetries responsible for neutrino mixing (112). The measurement of δ_{CP} is correlated to θ_{23} since, to leading order (Eq. (13)), the appearance probability depends on $\sin^2\theta_{23} \cdot \sin^2 2\theta_{13}$. Precision measurement of θ_{23} is therefore an important aspect of the current program. The accumulation of atmospheric and solar neutrino data is also expected to continue with Super-K, MINOS+, IceCube (115), and Borexino.

The main focus of the current program, however, is the $\nu_\mu \to \nu_e$ transition with the T2K and NOνA experiments. These experiments were both optimized before the discovery of θ_{13} to obtain evidence for this transition with the best signal to background ratio. The two principal backgrounds to an electron neutrino event in the few GeV range are: the intrinsic ν_e contamination present in the accelerator-produced beam at $\sim$ 1% level, and weak neutral current ν interactions that produce photons and π^0 particles. The ν_e background in the beam comes from μ and K-meson decays in the decay tunnel. The ν_e background is indistinguishable from the signal except that it has a broader energy spectrum. The neutral current processes produce photons from $\pi^0 \to \gamma\gamma$ decays that could be misidentified as single electrons in case of asymmetric or overlapping electro-magnetic showers. To limit the impact of both of these backgrounds with broad energy spectra, both T2K and NOνA have adapted the strategy of using a narrow neutrino energy spectrum. The narrow energy spectrum cuts down the contributions from neutrinos outside of the energies of interest as set by the oscillation probability. The narrow-band beam is achieved with the off-axis neutrino beam technique (44) in which the detector is placed at a small angle to the beam to exploit the kinematic momentum peak in the 2-body $\pi \to \mu\nu_\mu$ decay. The T2K and NOνA experiments utilize neutrino beams with a peak energy of $\sim$0.6 GeV and $\sim$2 GeV, at off-axis angles of 44 and 14 mrad, respectively.

The T2K experiment in Japan, running since 2010, has analyzed data from integrated exposure of 6.6×10^{20} protons with the beam polarity in the neutrino mode. The top plot in Fig. 7 shows the energy spectrum of 28 events identified as ν_e in T2K (116). The background expectation for these data from beam ν_e contamination and neutral current were 3.2 and 1.0 events, respectively. This observation conclusively establishes the presence of $\nu_\mu \to \nu_e$ oscillations driven by Δm^2_{31} at $> 7\sigma$ confidence level. The bottom panel of the figure shows the energy spectrum of the T2K ν_μ candidate events (117) compared to no oscillation expectation. The deficit of ν_μ in T2K is consistent with maximal mixing angle $\theta_{23} = \pi/4$. A combined fit using both appearance and disappearance data results in $\sin^2\theta_{23} \approx 0.52 \pm 0.07$ with a small dependence on the assumed mass hierarchy.

T2K has an excess of ν_e events compared to the prediction for $\delta_{CP} = 0$ and

the best fit value for $\sin^2\theta_{13}$ from reactor data. While T2K data alone cannot provide statistically significant constraints on δ_{CP}, the addition of the reactor measurement gives a preference for the negative values of δ_{CP} with the best-fit point near $-\pi/2$ (Fig. 10). Future addition of antineutrino data from T2K as well as the NOνA data should further constrain the parameter range.

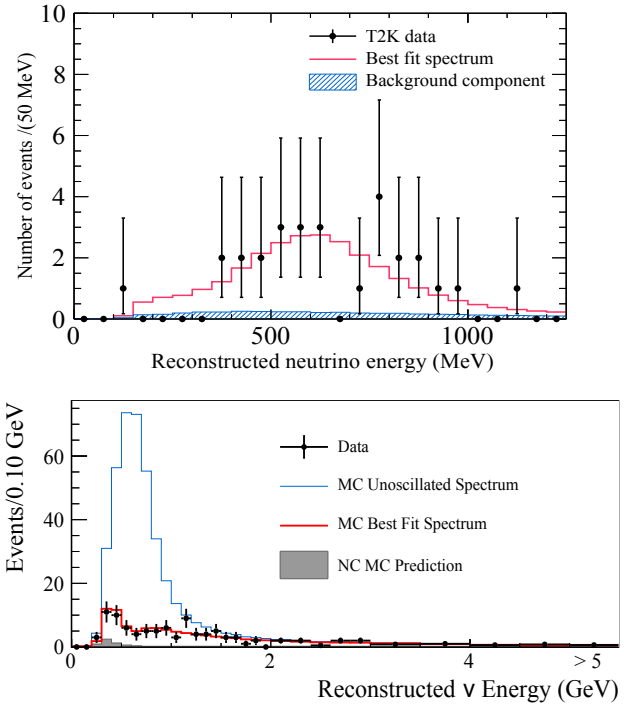

Figure 7: Top: Reconstructed energy spectrum of T2K ν_e candidate events (116) with expected backgrounds (blue) and the best-fit prediction under $\nu_\mu \to \nu_e$ oscillation hypothesis (red). Bottom: Reconstructed energy spectrum of T2K ν_μ candidate events (117) with the expectation under no-oscillation hypothesis (blue), background (gray), and the best-fit prediction (red).

The NOνA (NuMI Off-axis ν_e Appearance) experiment uses the Fermilab Main Injector 120 GeV proton beam. NOνA also follows the two-detector approach – both off-axis at 14 mrad – with the near detector (at 1 km) characterizing the neutrino beam close to the production point and the far (at 810 km) measuring the flavor composition after oscillations. The detectors use segmented liquid scintillator and are structurally and functionally identical with the near and far active masses of 0.3 and 14 kton, respectively. The NOνA collaboration reported their first measurement of ν_e appearance and ν_μ disappearance signals in the summer of 2015 (118) after 400 kW beam operation for about a year. Depending on the event reconstruction method, the experiment has found 6 to 11 ν_e events with background expectation of $\sim$ 1 event. The ν_e event rate appears to be consistent with $\delta_{CP} < 0$ with normal hierarchy and the disappearance result is consistent with the current picture of maximum mixing.

The size of the Earth matter effect depends on the energy of the oscillating neutrino (Eq. (6)). The T2K and NOνA experiments have the oscillation maximum at $\sim$ 0.6 and $\sim$ 1.6 GeV, respectively. The resulting large difference between

matter effects, since $N_e^{res} \propto 1/E_\nu$, provides complementarity between the two experiments. The increase (or suppression) of $P_{\mu e}$ due to the matter effect can be either masked or enhanced by the CP asymmetry, creating an ambiguity if the asymmetry due to matter is smaller than CP. The ambiguity can be reduced by a combination of measurements from the two experiments which will also provide information on the neutrino mass hierarchy and δ_{CP} (119).

5 Next-generation Experiments

The next generation experiments fall in two categories: detectors for high statistics atmospheric neutrino studies, and well-optimized experiments using man-made accelerator and reactor neutrinos. In both cases the detectors need to be very large with excellent energy resolution and particle identification, and well-shielded from cosmic ray muons.

5.1 Atmospheric Neutrinos

The next-generation atmospheric neutrino experiments will focus on resolving the neutrino mass hierarchy (MH) (120–124). In the normal (inverted) hierarchy there is a resonant effect for $\nu_\mu \to \nu_e$ ($\bar{\nu}_\mu \to \bar{\nu}_e$) at energy $E_\nu \sim 5$ GeV and zenith angle $\cos\theta \sim -0.85$ (corresponding to traversal through the outer core of the Earth). The effect can be measured through a large distortion in $P_{\mu\mu}$ and $P_{\bar{\mu}\bar{\mu}}$. Very large statistics (and correspondingly large detectors) are needed because of the limited solid angle and the atmospheric flux power law spectrum, $\sim 1/E^{2.7}$, in this energy range. The measurement requires excellent zenith angle resolution and an energy threshold $\lesssim 5$ GeV, relatively low for very large detectors optimized for very high energies (> 1 TeV) such as IceCube. The capability to differentiate positive and negative muons in a magnetized detector as well as muon tracks from showers allows increased sensitivity.

The proposed next-generation experiments include PINGU (125), ORCA (126), INO (127), and Hyper-Kamiokande (128). PINGU is a proposed multi-megaton high density array as an upgrade for IceCube at the South Pole Station. ORCA is proposed as a deep-sea neutrino telescope in the Mediterranean as part of KM3NeT (multi-km^3 neutrino telescope) (126). INO is a planned to be an underground magnetized iron calorimeter with $\sim$ 50 kton mass and 1.5 Tesla magnetic field in southern India. Hyper-Kamiokande (128) is a proposed giant water Cherenkov detector near the site of the current Super-Kamiokande detector in Japan. These experiments are expected to be limited by systematics because of the energy and angular resolution needed. Their capability to distinguish between the two mass hierarchies, which is correlated to θ_{23}, can reach above 3σ given enough exposure.

5.2 Reactor Neutrino Oscillations

The next generation reactor experiment will be optimized to resolve the mass hierarchy by detecting the $\sim \pm 3\%$ shift (Sec. 3) in energy dependent oscillations in the 2–8 MeV range. As usual the choice of the baseline distance is important. The fast oscillations due to the last two terms in Eq. (14) (Δ_{31} and Δ_{32}) will exhibit the shift at any distance, however at short distances (defined by $\Delta_{21} \ll \pi/2$), the

shift is ambiguous with the measurement of Δm^2_{31} itself, and at long distances ($\Delta_{21} \gg \pi/2$) the oscillations are too fast to be observable with achievable energy resolution. Using Eq. 14 we can write the asymmetry $P^{IH}(\bar{\nu}_e \to \bar{\nu}_e) - P^{NH}(\bar{\nu}_e \to \bar{\nu}_e)$ in obvious notation:

$$P^{IH}(\bar{\nu}_e \to \bar{\nu}_e) - P^{NH}(\bar{\nu}_e \to \bar{\nu}_e) = \sin^2 2\theta_{13} \cos^2 \theta_{12} \sin 2\Delta_{32} \sin 2\Delta_{21}. \quad (15)$$

At $\Delta_{21} = \pi/2$ or the maximum of solar oscillations, the asymmetry between IH and NH vanishes. For $\Delta_{21} < \pi/2$, the $P_{\bar{e}\bar{e}}$ oscillations are shifted to lower (higher) energies for normal (inverted) hierarchy, but for $\Delta_{21} > \pi/2$, the converse is true. This phenomenology allows us to choose L so that the $\Delta_{21} = \pi/2$ node is around ~ 3 MeV or the maximum of the reactor spectrum to avoid ambiguities (107). This node can be shown to be at $L = 2\pi E/\Delta m^2_{21} \approx 50$ km. The oscillations on either side of the node at ~ 3 MeV can be compared in a single detector to resolve for IH versus NH, reducing dependence on the absolute energy calibration (Fig. 8). Nevertheless, the detector must have sufficient statistics ($\sim 10^5$ events after oscillations), energy resolution($\lesssim 3\%$ at 1 MeV), and linearity ($\lesssim 1\%$) across the reactor energy range. Otherwise, low-energy oscillation pattern will be smeared out. The detector also must be equidistant from all reactor cores so that the oscillation pattern is not obscured. The large event sample from such an arrangement would also enable precision ($\sim 1\%$) measurements of $\sin^2 2\theta_{12}$, Δm^2_{21}, and Δm^2_{32}.

There are two proposed next generation reactor experiments: the Jiangmen Underground Neutrino Observatory (JUNO) (129, 130) in China and RENO-50 (131) in South Korea. JUNO (RENO-50) design calls for a 20 kton (18 kton) fiducial mass liquid scintillator detector placed 700 m (900 m) underground, 52.5 km (47 km) away from a set of reactors with total thermal power of ~ 36 GW (~ 16 GW). At about 50 km, the IBD rate is $\sim 0.1(0.3)$ day^{-1}kton^{-1}GW^{-1} with (without) oscillations indicating a need for ~3000 kton·GW·year of exposure.

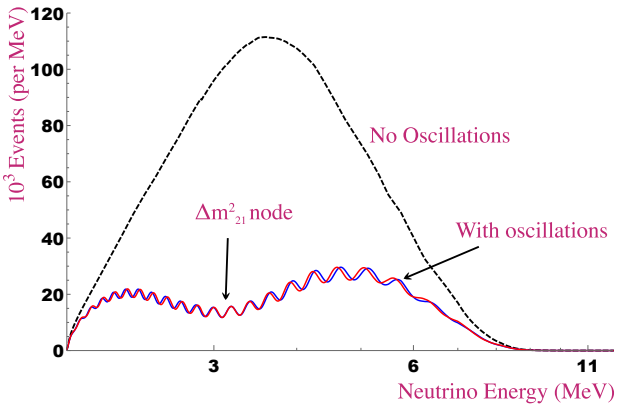

Figure 8: Reactor antineutrino spectrum is shown at 52.5 km for no oscillations (dashed)(23, 24), and for $\Delta m^2_{32} = +2.4 \times 10^{-3}$eV^2 (red) for NH and -2.4×10^{-3}eV^2(blue) for IH. The event rate is normalized to 3000 kton·GW·year. To demonstrate the principle of the experiment no energy smearing is included.

The needed energy resolution and linearity lead to requirements on the scintillator brightness, attenuation length, photo-detector coverage, and quantum efficiency so that the photo-electron yield is $\gtrsim 1000$ per MeV. With the required

energy resolution JUNO will achieve $> 3\sigma$ separation of the two mass hierarchies with ∼6 years of operation(130).

5.3 Accelerator Neutrino Oscillations

Precision studies of neutrino oscillations with accelerators will focus on the search for CP violation with an optimized combination of neutrino beam energy, distance to the detector, and detector technology. The preferred mode for future accelerator studies is $\nu_\mu \to \nu_e$ and the charge conjugate $\bar{\nu}_\mu \to \bar{\nu}_e$ (See Sec.3); this requires production of an intense broadband ν_μ ($\bar{\nu}_\mu$) beam. Using the known parameter values the expected size of the signal at first maximum is $\sin^2\theta_{23}\sin^2 2\theta_{13} \approx 5\%$, well above the the contamination ν_e background of $\sim$ 1% in a horn focused beam. Therefore alternative methods using very pure intense beams of ν_e and $\bar{\nu}_e$ using μ decay such as the Neutrino Factory (132, 133) or decays of radioactive beta beams (134) are no longer favored.

The asymmetry $A^{\mu e}$ has contributions from CP violation of $\leq$ 32%, and from the matter effect which grows as a function of the oscillation energy (or the length of baseline) as $\sim \pm 2N_e/N_e^{res}$, with the sign dependent on MH. At the first oscillation maximum, $\Delta_{31} \cong \Delta_{32} = \pi/2$, the asymmetry due to matter effect exceeds the maximum from CP violation at $E_\nu \sim$ 2.3 GeV or ∼ 1200 km (91,135). Therefore, two different strategies for experimental optimization exist: distances of $\lesssim$ 500 km would allow measurement of CP violation with low dependence on MH, while distances of $\gtrsim$ 1200 km would allow resolution of MH and also be sensitive to CP violation. A minimum distance is determined from the requirement that $E_\nu \gtrsim 0.5$ GeV, a condition that ensures high enough probability for ν and $\bar{\nu}$ interactions and good particle reconstruction and identification. An additional consideration is to obtain events at the second oscillation maximum, $\Delta_{32} = 3\pi/2$ where CP effects are a factor of 3 larger, but event rate is ∼ 9 times smaller due to kinematics. A broadband beam designed for baselines of $\gtrsim$ 1200km will also have sensitivity at second maximum (92,135), an important consideration in resolving ambiguities.

The expected event rate for a broadband beam can be calculated to lowest order by integrating the muon neutrino flux, $\Phi(E_\nu) \cong C/L^2$ with L in km and $C \sim 10^{17}$ $\nu_\mu/\mathrm{m}^2/\mathrm{GeV}/\mathrm{MW}/\mathrm{yr}$ with the appearance probability $P_{\mu e}$, and the charged current cross section $\sigma(E_\nu) \cong 0.7 \times 10^{-38} E_\nu$ cm^2/GeV/nucleon. For vacuum oscillations the event rate is found to be independent of the baseline distance because of the increase of oscillation probability and the cross section so that $N_{\nu_\mu \to \nu_e}(L) \sim \mathcal{O}(20)\mathrm{events}/(\mathrm{kt}\cdot\mathrm{MW}\cdot\mathrm{yr})$, with the rate for $\bar{\nu}$ approximately 1/3 of ν. For off-axis beams and distances $\lesssim$ 500 km, the event yield and the ratio of $\bar{\nu}/\nu$ events is smaller. For most modern high energy accelerators, the available beam power is limited to $\lesssim$ 1 MW(136), therefore detectors with efficient mass (mass times efficiency) of $\gtrsim$ 50 kton are needed independent of distance to obtain a few hundred ν_e appearance events. At such large scales, water Cherenkov and liquid argon time projection chambers are considered cost effective technologies (137, 138). At low energies ($\lesssim$ 1 GeV)– distances of $\lesssim$ 500 km – the charged current ν_e cross section is dominated by quasielastic interactions with low multiplicity final states, well-reconstructed by water Cherenkov detectors. However, at higher energies ($\gtrsim$ 2 GeV) – distances of $\gtrsim$ 1000 km – charged current events with multiple final state particles must be reconstructed to retain high efficiency; a high granularity detector such as a liquid argon time projection

chamber is therefore preferred.

The Hyper-Kamiokande (Hyper-K) experiment (128) in Japan with a baseline of 295 km and the Deep Underground Neutrino Experiment (DUNE) at the Long-Baseline Neutrino Facility (LBNF) in the U.S. with a baseline of $\sim$ 1300 km (138–140) have chosen the two complementary approaches as outlined above.

Hyper-K is planned to be a water Cherenkov detector with 560 kton (1 Mton) fiducial (total) mass near the current Super-K site in western Japan at a depth of $\sim$ 650 m. The Hyper-K detector will be placed in the same 44 mrad off-axis neutrino beam matched to the first oscillation node (Fig. 9) as T2K but with a much larger detector and beam power of $\sim$ 1.3 MW. Hyper-K will also have a complex of near detectors to monitor and measure the beam to predict background and signal rates at the far detector.

DUNE consists of a horn-produced broad band beam with 60-120 GeV protons with beam-power of $\sim$1.2 MW from Fermilab, 40 kton fiducial volume liquid argon time projection far detector $\sim$1450 m underground at Sanford Underground Research Laboratory in South Dakota, and high-resolution near detector (140). The baseline of DUNE (91, 139) is $\sim$1300 km which is optimized to measure the matter effect and CP violation simultaneously. The DUNE broad-band flux (Fig. 9) is designed to cover the first ($\sim$ 2.5 GeV) and second ($\sim$ 0.8 GeV) oscillation nodes sufficiently so that the CP phase can be measured using the distortion of the energy spectrum as well as the $\nu, \bar{\nu}$ asymmetry.

The liquid argon time projection technology (141–143), chosen for DUNE, could be implemented by two approaches: the single phase in which the drifting charge is detected by electrodes in the liquid argon (139) or the double phase in which the charge is drifted to the surface of the liquid argon and amplified in the gas phase before detection (135).

The Hyper-K and DUNE experiments require precise prediction of ν_e signal and background spectra in the far detector. The prediction is calculated by extrapolating the measured event spectrum from the near detector, using the known beam geometry and constraints on the cross sections, and near and far detector efficiencies. The systematic errors associated with neutrino nucleus cross sections require further measurements and modeling (144). Since the maximum expected asymmetry from CP violation is 32%, the requirement on the allowed systematic error is less than a few percent so that a 5σ effect can be measured with $\mathcal{O}(1000)$ events. A joint fit to the four spectra – ν_μ, $\bar{\nu}_\mu$, ν_e, $\bar{\nu}_e$ – is expected to cancel some uncertainties, and the remaining largest contribution is expected to come from the relative energy scale for ν_e and ν_μ events (145). For DUNE, if the matter and CP asymmetries have the same sign, the combined effect is very large and the mass hierarchy will be determined to $> 5\sigma$ within a few months of running; in case of the opposite, exposure of a few years is needed (139). Figure 10 shows the current global fit for δ_{CP} versus $\sin^2 2\theta_{13}$ while marginalizing over all other oscillation parameters (29,30) including the reactor constraint on θ_{13}. The figure also shows the expectation at $\delta_{CP} = 0$ and $\pm\pi/2$ for Hyper-K (DUNE) assuming 10 yrs of exposure at 1.3 MW (1.2 MW) (140, 146). The Hyper-K and DUNE expectations do not include the θ_{13} constraint. The independent measurements of θ_{13} from accelerators and reactors can be compared to test for new physics (83).

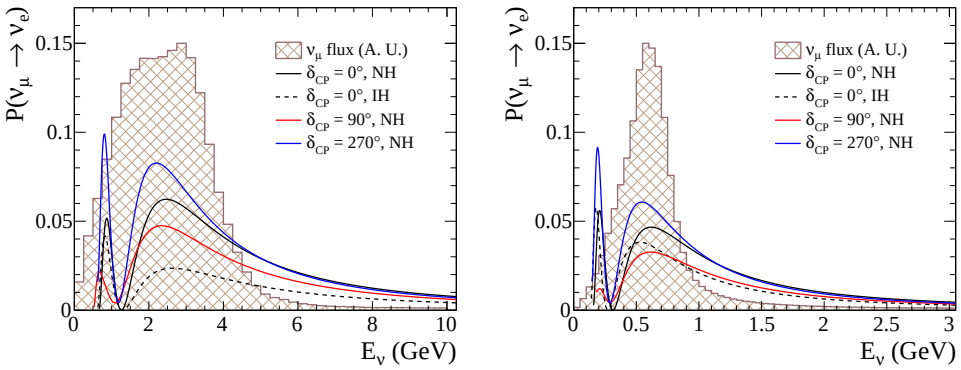

Figure 9: $P(\nu_\mu \to \nu_e)$ plotted as a function of energy for 1300 km and 295 km with the neutrino spectrum designed for DUNE (left) and Hyper-K (right) in arbitrary units. The probability for antineutrinos will be modified approximately by $\delta_{CP} \to -\delta_{CP}$ and NH→IH. The antineutrino spectrum shape is approximately the same.

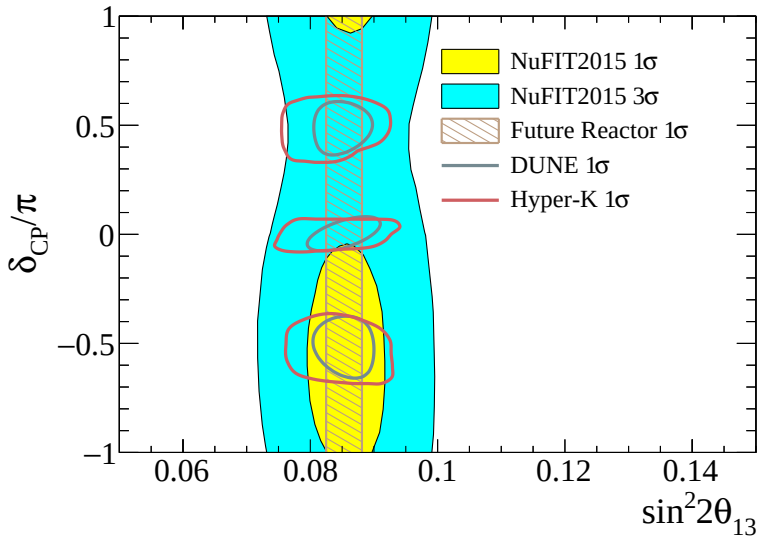

Figure 10: Current measurements and future goals in the δ_{CP} and $\sin^2 2\theta_{13}$ plane. The current best fit in yellow (cyan) for 1σ (3σ) C.L. is from a combination of T2K and reactor measurements. Brown vertical band shows the future reactor measurement dominated by Daya Bay. The blue-gray (maroon) contours show measurements that could result from DUNE (Hyper-K) at δ_{CP} values of $\pm 90°$ and $0°$. The Hyper-K and DUNE projections are taken from Ref. (146) and Ref. (140), respectively. Hyper-K and DUNE do not have identical treatment of the correlation to θ_{23}. For Hyper-K the mass hierarchy is assumed to be known; for DUNE the measurement can be done with the same data.

6 Conclusion

We have reviewed the current status of the physics of long-baseline neutrino oscillations with emphasis on the experimental technique. The picture of 3-flavor

oscillations has now been established by observation of neutrino oscillations with solar, atmospheric, reactor, and accelerator neutrinos. Remarkably, a consistent picture of mass differences and mixing has emerged so that extremely precise experiments, using well-characterized and controlled terrestrial sources of neutrinos using reactors and accelerators, are now feasible. The main objectives of such an experimental program are the determination of potentially large CP violation in the neutrino sector, resolution of the mass ordering, and measurement of the mixing parameters with greater precision. The precision and redundancy of measurements will allow constraints on new physics beyond the 3-flavor model as well as neutrino mass and mixing models.

This work was supported by the U.S. Department of Energy, the Swiss National Science Foundation (SNF), and the French National Centre for Scientific Research (CNRS).

Literature Cited

1. Brown LM, Physics Today 31:23 (1978).
2. Fermi E, Il Nuovo Cimento 11:1 (1934).
3. Reines F, Cowan CL, Nature 178:446 (1956).
4. Cowan CL, Reines F, Harrison FB, Kruse HW, McGuire AD, Science 124:103 (1956).
5. Winter K, Neutrino Physics (Cambridge Uni. Pr., 2000).
6. Kolb EW, Turner MS, The Early Universe (Westview Pr., 1990).
7. Part. Data Group, Olive KA, et al., Chin. Phys. C38:090001 (2014).
8. Mohapatra RN, et al., Rept. Prog. Phys. 70:1757 (2007), hep-ph/0510213.
9. Pontecorvo B, Zh. Eksp. Theor. Phys. 33:549 (1957).
10. Pontecorvo B, Sov. Phys. JETP 6:429 (1958).
11. Pontecorvo B, Zh. Eksp. Theor. Phys. 53:1717 (1967).
12. Pontecorvo B, Sov. Phys. JETP 26:989 (1967).
13. Maki Z, Nakagawa M, Sakata S, Prog. Theor. Phys. 28:247 (1962).
14. Danby G, Gaillard JM, Goulianos KA, Lederman LM, Mistry NB, et al., Phys. Rev. Lett. 9:36 (1962).
15. Akhmedov EK, Smirnov AYu, Phys. Atom. Nucl. 72:1363 (2009), 0905.1903.
16. Commins ED, Bucksbaum PH, Weak Interactions of Leptons and Quarks (Cambridge Univ. Pr., 1983).
17. Wolfenstein L, Phys. Rev. D17:2369 (1978).
18. Mikheev SP, Smirnov AYu, Sov. J. Nucl. Phys. 42:913 (1985), [Yad. Fiz.42,1441(1985)].
19. Barger VD, Whisnant K, Pakvasa S, Phillips RJN, Phys. Rev. D22:2718 (1980).
20. Renga F, (2012), 1208.3593.
21. Otten EW, Weinheimer C, Rept. Prog. Phys. 71:086201 (2008), 0909.2104.
22. Haxton WC, Hamish Robertson RG, Serenelli AM, Ann. Rev. Astron. Astrophys. 51:21 (2013), 1208.5723.
23. Mueller TA, et al., Phys. Rev. C83:054615 (2011), 1101.2663.
24. Huber P, Phys. Rev. C84:024617 (2011), 1106.0687, [Erratum: Phys. Rev.C85,029901(2012)].
25. Gaisser TK, Honda M, Ann. Rev. Nucl. Part. Sci. 52:153 (2002), hep-ph/0203272.

26. Honda M, Kajita T, Kasahara K, Midorikawa S, Phys. Rev. D83:123001 (2011), 1102.2688.
27. Suzuki Y, Nakahata M, Moriyama S, Koshio Y, eds., Neutrino oscillations and their origin. Proceedings, 5th International Workshop, NOON2004, Tokyo, Japan, February 11-15, 2004, 2005.
28. Dusseux JC, Pattison JBM, Ziebarth G, The cern magnetic horn (1971) and its remote-handling system., CERN-72-11 June 1972.
29. Gonzalez-Garcia MC, Maltoni M, Schwetz T, JHEP 11:052 (2014), 1409.5439.
30. Forero D, Tortola M, Valle J, (2014), 1405.7540.
31. Mena O, Parke SJ, Phys. Rev. D69:117301 (2004), hep-ph/0312131.
32. Super-Kamiokande Collab., Fukuda Y, et al., Nucl. Instrum. Meth. A501:418 (2003).
33. Super-Kamiokande Collab., Fukuda Y, et al., Phys. Rev. Lett. 81:1562 (1998), hep-ex/9807003.
34. Kamiokande Collab., Hatakeyama S, et al., Phys. Rev. Lett. 81:2016 (1998), hep-ex/9806038.
35. Clark R, et al., Phys. Rev. Lett. 79:345 (1997).
36. Kajita T, Ann. Rev. Nucl. Part. Sci. 64:343 (2014).
37. Super-Kamiokande Collab., Ashie Y, et al., Phys. Rev. Lett. 93:101801 (2004), hep-ex/0404034.
38. K2K Collab., Ahn MH, et al., Phys. Rev. D74:072003 (2006).
39. MINOS Collab., Adamson P, et al., Phys. Rev. Lett. 110:251801 (2013).
40. T2K Collab., Abe K, et al., Phys. Rev. Lett. 111:211803 (2013), 1308.0465.
41. MINOS Collab., Adamson P, et al., Phys. Rev. Lett. 112:191801 (2014), 1403.0867.
42. T2K Collab., Abe K, et al., Phys. Rev. Lett. 112:181801 (2014), 1403.1532.
43. MINOS Collab., Adamson P, et al., Phys. Rev. D77:072002 (2008), 0711.0769.
44. E889 Collab., Beavis D, et al., Brookhaven National Laboratory Report No. BNL-52459, 1995 (unpublished), www.osti.gov No. 52878.
45. T2K Collab., Abe K, et al., Nucl. Instrum. Meth. A659:106 (2011), 1106.1238.
46. Super-Kamiokande Collab., Abe K, et al., Phys. Rev. Lett. 110:181802 (2013).
47. Yoshida J, et al., JINST 8:P02009 (2013).
48. OPERA Collab., Agafonova N, et al., Phys. Rev. Lett. 115:121802 (2015), 1507.01417.
49. OPERA Collab., Agafonova N, et al., Phys. Rev. D 89:051102 (2014).
50. MINOS Collab., Adamson P, et al., Phys. Rev. Lett. 110:251801 (2013), 1304.6335.
51. Cleveland BT, Daily T, Davis Jr. R, Distel JR, Lande K, et al., Astrophys. J. 496:505 (1998).
52. Bahcall JN, Pinsonneault MH, Basu S, Astrophys. J. 555:990 (2001), astro-ph/0010346.
53. SAGE Collab., Abdurashitov JN, et al., Phys. Rev. C60:055801 (1999), astro-ph/9907113.
54. GALLEX Collab., Hampel W, et al., Phys. Lett. B447:127 (1999).
55. Kamiokande Collab., Fukuda Y, et al., Phys. Rev. Lett. 77:1683 (1996).
56. Super-Kamiokande Collab., Fukuda Y, et al., Phys. Rev. Lett. 81:1158

(1998), hep-ex/9805021, [Erratum: Phys. Rev. Lett.81,4279(1998)].
57. Super-Kamiokande Collab., Fukuda S, et al., Phys. Lett. B539:179 (2002), hep-ex/0205075.
58. SNO Collab, Aharmim B, et al., Phys. Rev. C72:055502 (2005), nucl-ex/0502021.
59. SNO Collab., Ahmad QR, et al., Phys. Rev. Lett. 89:011301 (2002), nucl-ex/0204008.
60. Bonventre R, LaTorre A, Klein JR, Orebi Gann GD, Seibert S, Wasalski O, Phys. Rev. D88:053010 (2013), 1305.5835.
61. Mikheyev SP, Smirnov AY, Sov. J. Nucl. Phys. 42:913 (1986).
62. Mikheyev SP, Smirnov AY, Sov. Phys. JETP 64:4 (1986).
63. Mikheyev SP, Smirnov AY, Nuovo Cim 9C:17 (1986).
64. KamLAND Collab., Eguchi K, et al., Phys. Rev. Lett. 90:021802 (2003), hep-ex/0212021.
65. KamLAND Collab., Gando A, et al., Phys. Rev. D88:033001 (2013), 1303.4667.
66. Fogli GL, Lisi E, Marrone A, Palazzo A, Rotunno AM, Phys. Rev. D84:053007 (2011), 1106.6028.
67. Chooz Collab., Apollonio M, et al., Phys.Lett. B466:415 (1999), hep-ex/9907037.
68. Chooz Collab., Apollonio M, et al., Eur.Phys.J. C27:331 (2003), hep-ex/0301017.
69. Boehm F, Busenitz J, Cook B, Gratta G, Henrikson H, et al., Phys.Rev. D64:112001 (2001), hep-ex/0107009.
70. Double-Chooz Collab., Abe Y, et al., Phys.Rev.Lett. 108:131801 (2012), 1112.6353.
71. Daya-Bay Collab., An F, et al., Phys.Rev.Lett. 108:171803 (2012), 1203.1669.
72. RENO Collab., Ahn J, et al., Phys.Rev.Lett. 108:191802 (2012), 1204.0626.
73. Daya-Bay Collab., An FP, et al., Chin. Phys. C37:011001 (2013), 1210.6327.
74. Daya-Bay Collab., An FP, et al., Phys. Rev. Lett. 115:111802 (2015), 1505.03456.
75. MINOS Collab., Adamson P, et al., Phys.Rev.Lett. 107:181802 (2011), 1108.0015.
76. T2K Collab., Abe K, et al., Phys.Rev.Lett. 107:041801 (2011), 1106.2822.
77. Qian X, Vogel P, Prog. Part. Nucl. Phys. 83:1 (2015), 1505.01891.
78. Aguilar-Arevalo A, et al., Phys. Rev. D64:112007 (2001).
79. MiniBooNE Collab., Aguilar-Arevalo A, et al., Phys.Rev.Lett. 110:161801 (2013), 1207.4809.
80. Mention G, et al., Phys. Rev. D83:073006 (2011).
81. Abazajian KN, et al., (2012), 1204.5379.
82. Antusch S, et al., JHEP 0610:084 (2006).
83. Qian X, Zhang C, Diwan M, Vogel P, (2013), 1308.5700.
84. Fukugita M, Yanagida T, Phys. Lett. B174:45 (1986).
85. Abada A, Davidson S, Josse-Michaux FX, Losada M, Riotto A, JCAP 0604:004 (2006), hep-ph/0601083.
86. Nardi E, Nir Y, Roulet E, Racker J, JHEP 01:164 (2006), hep-ph/0601084.
87. Pascoli S, Petcov ST, Riotto A, Phys. Rev. D75:083511 (2007), hep-ph/0609125.
88. Pascoli S, Petcov ST, Riotto A, Nucl. Phys. B774:1 (2007), hep-ph/0611338.

89. Marciano WJ, (2001), hep-ph/0108181.
90. Parke SJ, Theta(13), in Particles and nuclei : Seventeenth International Conference on Particles and Nuclei, Santa Fe, New Mexico, 23-30 October 2005, 2005.
91. LBNE Collab., Bass M, et al., Phys. Rev. D91:052015 (2015), 1311.0212.
92. Diwan MV, et al., Phys. Rev. D68:012002 (2003), hep-ph/0303081.
93. Chizhov MV, Petcov ST, Phys. Rev. D63:073003 (2001), hep-ph/9903424.
94. Akhmedov EK, Maltoni M, Smirnov AYu, JHEP 05:077 (2007), hep-ph/0612285.
95. Freund M, Phys. Rev. D64:053003 (2001), hep-ph/0103300.
96. Diwan MV, Frascati Phys. Ser. 35:89 (2004), hep-ex/0407047, [,89(2004)].
97. Daya-Bay Collab., An FP, et al., Phys. Rev. Lett. 112:061801 (2014), 1310.6732.
98. RENO Collab., (2015), 1511.05849.
99. Petcov ST, Piai M, Phys. Lett. B533:94 (2002), hep-ph/0112074.
100. Choubey S, Petcov ST, Piai M, Phys. Rev. D68:113006 (2003), hep-ph/0306017.
101. de Gouvea A, Jenkins J, Kayser B, Phys. Rev. D71:113009 (2005), hep-ph/0503079.
102. Learned J, Dye ST, Pakvasa S, Svoboda RC, Phys. Rev. D78:071302 (2008), hep-ex/0612022.
103. Minakata H, Nunokawa H, Parke SJ, Zukanovich Funchal R, Phys. Rev. D76:053004 (2007), hep-ph/0701151, [Erratum: Phys. Rev.D76,079901(2007)].
104. Parke SJ, Minakata H, Nunokawa H, Funchal RZ, Nucl. Phys. Proc. Suppl. 188:115 (2009), 0812.1879.
105. Zhan L, Wang Y, Cao J, Wen L, Phys. Rev. D78:111103 (2008), 0807.3203.
106. Zhan L, Wang Y, Cao J, Wen L, Phys. Rev. D79:073007 (2009), 0901.2976.
107. Qian X, Dwyer DA, McKeown RD, Vogel P, Wang W, Zhang C, Phys. Rev. D87:033005 (2013), 1208.1551.
108. Ciuffoli E, Evslin J, Zhang X, JHEP 03:016 (2013), 1208.1991.
109. Ge SF, Hagiwara K, Okamura N, Takaesu Y, JHEP 05:131 (2013), 1210.8141.
110. Li YF, Cao J, Wang Y, Zhan L, Phys. Rev. D88:013008 (2013), 1303.6733.
111. Minakata H, Smirnov AYu, Phys. Rev. D70:073009 (2004), hep-ph/0405088.
112. Altarelli G, Feruglio F, Rev. Mod. Phys. 82:2701 (2010), 1002.0211.
113. Timmons A, (2015), 1511.06178.
114. Daya-Bay Collab., Zhang C, AIP Conf. Proc. 1666:080003 (2015), 1501.04991.
115. IceCube Collab., Aartsen M, et al., Phys. Rev. D91:072004 (2015), 1410.7227.
116. T2K Collab., Abe K, et al., Phys. Rev. Lett. 112:061802 (2014), 1311.4750.
117. T2K Collab., Abe K, et al., Phys. Rev. D91:072010 (2015), 1502.01550.
118. R. B. Patterson, JETP Seminar at Fermilab, `http://nova-docdb.fnal.gov/cgi-bin/ShowDocument?docid=13883`.
119. T2K Collab., Abe K, et al., PTEP 2015:043C01 (2015), 1409.7469.
120. Franco D, Jollet C, Kouchner A, Kulikovskiy V, Meregaglia A, et al., JHEP 04:008 (2013), 1301.4332.
121. Ribordy M, Smirnov AY, Phys. Rev. D87:113007 (2013), 1303.0758.
122. Winter W, Phys. Rev. D88:013013 (2013), 1305.5539.

123. Ge SF, Hagiwara K, JHEP 09:024 (2014), 1312.0457.
124. Capozzi F, Lisi E, Marrone A, Phys. Rev. D91:073011 (2015), 1503.01999.
125. IceCube-PINGU Collab., Aartsen M, et al., (2014), 1401.2046.
126. KM3NeT Collab., Katz UF, Submitted to: PoS (2014), 1402.1022.
127. ICAL Collab., Ahmed S, et al., (2015), 1505.07380.
128. Hyper-Kamiokande Working Group, Abe K, et al., A Long Baseline Neutrino Oscillation Experiment Using J-PARC Neutrino Beam and Hyper-Kamiokande, 2014, 1412.4673.
129. JUNO Collab., Djurcic Z, et al., (2015), 1508.07166.
130. JUNO Collab., An F, et al., (2015), 1507.05613.
131. Kim SB, Nucl. Part. Phys. Proc. 265:93 (2015), 1412.2199.
132. IDS-NF Consortium, Choubey S, et al., (2011), 1112.2853.
133. Geer S, Phys. Rev. D57:6989 (1998), hep-ph/9712290, [Erratum: Phys. Rev.D59,039903(1999)].
134. Wildner E, et al., Phys. Rev. ST Accel. Beams 17:071002 (2014).
135. LAGUNA-LBNO Collab., Agarwalla SK, et al., JHEP 05:094 (2014), 1312.6520.
136. Henderson S, ed., High-intensity, high-brightness hadron beams. Proceedings, 42nd Advanced Beam Dynamics Workshop, ABDW-HB'08, Nashville, USA, August 25-29, 2008, 2008.
137. Barger V, et al., (2007), 0705.4396.
138. LAGUNA Consortium, Rubbia A, Acta Phys. Polon. B41:1727 (2010).
139. LBNE Collab., Adams C, et al., (2013), 1307.7335.
140. DUNE, Acciarri R, et al., (2015), 1512.06148.
141. Willis WJ, Radeka V, Nucl. Instrum. Meth. 120:221 (1974).
142. Nygren DR, eConf C740805:58 (1974).
143. Rubbia C, The liquid-argon time projection chamber: A new concept for neutrino detector, CERN-EP/77-08 (1977).
144. Mosel U, Ann. Rev. Nucl. Part. Sci. 66 (2016).
145. Szczerbinska B, Worcester E, eds., Proceedings, Workshop on Neutrino Interactions, Systematic uncertainties and near detector physics: Session of CETUP* 2014, volume 1680, 2015.
146. Hyper-Kamiokande Collab., Abe K, et al., PTEP 2015:053C02 (2015), 1502.05199.